

Markov-type state models to describe non-Markovian dynamics

Sofia Sartore, Franziska Teichmann, and Gerhard Stock*

Biomolecular Dynamics, Institute of Physics, University of Freiburg, 79104 Freiburg, Germany

E-mail: stock@physik.uni-freiburg.de

Abstract

When clustering molecular dynamics (MD) trajectories into a few metastable conformational states, the assumption of timescale separation between fast intrastate fluctuations and rarely occurring interstate transitions is often not valid. Hence, when we construct a Markov state model (MSM) from these states, the naive estimation of the macrostate transition matrix via simply counting transitions between the states may lead to significantly too short implied timescales and thus to too fast population decays. In this work, we discuss advanced approaches to estimate the transition matrix. Assuming that Markovianity is at least given at the microstate level, we consider the Laplace-transform based method by Hummer and Szabo, as well as a direct microstate-to-macrostate projection, which by design yields correct macrostate population dynamics. Alternatively, we study the recently proposed quasi-MSM ansatz of Huang and coworkers to solve a generalized master equation, as well as a hybrid method that employs MD at short times and MSM at long times. Adopting a one-dimensional toy model and an all-atom folding trajectory of HP35, we discuss the virtues and shortcomings of the various approaches.

1 Introduction

Classical molecular dynamics (MD) simulations are a versatile tool for gaining insights into complex biomolecular processes.¹ To facilitate the interpretation of the ever-increasing amount of data obtained from such simulations, coarse grained models such as Langevin equations²⁻⁴ and Markov state models⁵⁻⁸ (MSMs) can be useful. Interpreting MD trajectories in terms of memoryless transitions between metastable conformational states, MSMs are popular because they provide a generally accepted state-of-the-art analysis, promise to predict long-time dynamics from short trajectories, and are straightforward to build using open-source packages.⁹⁻¹¹ The usual workflow to construct an MSM consists of (i) selection of suitable input coordinates or features, (ii) dimensionality reduction from the high-dimensional feature space to some low-dimensional space of collective variables, (iii) geometrical clustering of these low-dimensional data into microstates, (iv) dynamical clustering of the microstates into metastable conformational states (or macrostates), and (v) estimation of the transition matrix associated with these states.

Here, we are concerned with the last step of the procedure, that is, we want to discuss various approaches (and propose new ways) to estimate the macrostate transition matrix $\mathbf{T}(t)$. Since these formulations may go beyond the scope of a common MSM, we call them 'Markov-type state

models.' In what follows, we assume that steps (i) - (iv) resulted in a partitioning of N macrostates, such that the MD data can be converted to a state trajectory $I(t)$. Moreover we assume that all states are connected such that the MSM is ergodic, and that the MD data represent a stationary and time-homogeneous process. To focus on the effects of non-Markovianity, we for now also assume sufficient sampling of the MD data (but see Sec. 3.2).

The macrostate transition matrix $\mathbf{T}(t)$ contains the probabilities T_{IJ} that the system jumps from state J to state I within some pre-chosen lag time, which can be obtained by simply counting the transitions from J to I within t . When we denote the time-dependent state vector by $\mathbf{P}(t) = (P_1, \dots, P_N)^T$ with state probabilities P_I , the time evolution of the state model can be written as

$$\mathbf{P}(t) = \mathbf{T}(t)\mathbf{P}(0). \quad (1)$$

We note that the time-dependent transition matrix $\mathbf{T}(t)$ does not involve a dynamical approximation (such as the Markov approximation discussed below), but is directly obtained from the MD data. As a consequence, its practical use is limited by the fact that the calculation of $\mathbf{T}(t)$ is restricted to times $t \lesssim t_{\max}$, where t_{\max} is the length of the MD trajectories. That is, Eq. (1) is in essence a state representation of the dynamics, but it does not allow any prediction beyond the timescale of the MD simulations.

The latter can be achieved by invoking a Markov approximation, which assumes a timescale separation between fast intrastate fluctuations and rarely occurring interstate transitions. Assuming that the intrastate fluctuations randomize for times longer than some specific lag time τ , we expect that the transition matrix $\mathbf{T}(t)$ becomes constant for $t \gtrsim \tau$. Hence, $\mathbf{T}(t)$ can be approximated by

$$\mathbf{T}(t=m\tau) \approx \mathbf{T}^m(\tau) \quad (2)$$

with $m = 1, 2, \dots$, which only requires short MD trajectories (in principle as short as τ) to estimate the transition matrix. Since the time evolution of the MSM is given in steps of τ , the lag time defines the time resolution of the model, and therefore needs to be chosen shorter than the fastest dynamics of interest. This condition, however, is often in conflict with the above requirement of a long enough lag time to achieve Markovianity of the system, i.e., a constant transition matrix. Therefore, in practice one often ends up with a state partitioning that is only approximately Markovian at the desired time resolution, which raises the question of the optimal MSM that best approximates the dynamics in this case.

There are various ways to compute the MSM transition matrix $\mathbf{T}(\tau)$, in order to optimize the approxima-

tion of the true transition matrix $\mathbf{T}(t)$ in Eq. (2). For one, we may go beyond the simple counting scheme mentioned above and invoke our knowledge of the microstates the macrostates are built of.¹²⁻¹⁵ This approach exploits that microstates are typically structurally homogeneous, and therefore require only a relatively short lag time to randomize and show Markovian behavior. Macrostates, on the other hand, typically contain numerous structurally different microstates that may be separated by free energy barriers, resulting in long lag times to reach Markovianity. Along these lines, Hummer and Szabo¹³ proposed a valuable formulation to optimally project the microstate dynamics onto the macrostate dynamics, which was shown to achieve significantly improved Markovianity.

Alternatively, we may consider an (in principle) exact equation of motion for the time-dependent state vector $\mathbf{P}(t)$.¹⁶⁻²⁰ By employing projection operator techniques, Zwanzig¹⁶ derived the generalized master equation

$$\frac{d\mathbf{P}(t)}{dt} = \int_0^t \mathbf{K}(t')\mathbf{P}(t-t') dt', \quad (3)$$

where $\mathbf{K}(t)$ is the memory kernel matrix that accounts for the non-Markovian dynamics of the system. To obtain an equation of motion for the transition matrix, we may replace $\mathbf{P}(t)$ by $\mathbf{T}(t)$ using Eq. (1). While the estimation of the memory kernel for (typically noisy and under-sampled) MD data represents a non-trivial task,²¹⁻²³ Huang and coworkers¹⁷ recently proposed a promising method termed quasi-MSM (qMSM), which was successfully applied to various systems.^{24,25} We also wish to mention a simpler but often effective way of taking memory into account. By ‘coring’ the macrostate trajectory, we either request that a transition from one state to another must reach some pre-defined core region of the other state,^{5,26,27} or that the system spends a certain minimum time in the new state.²⁸ The latter approach, termed ‘dynamical coring’ was shown to considerably improve the Markovianity of the resulting metastable states.²⁹

In this work, we discuss the theoretical basis and the performance of various approaches to estimate $\mathbf{T}(t)$, including the Hummer-Szabo projection,¹³ the qMSM ansatz of Huang and coworkers,¹⁷ and two new approaches termed ‘microstate-based’ and ‘hybrid MD/MSM’ method, respectively. Adopting a one-dimensional toy model and an all-atom folding trajectory of HP35,³⁰ we discuss the applicability as well as the virtues and shortcomings of these approaches.

2 Theory and Methods

To estimate the macrostate transition matrix \mathbf{T} , we consider three complementary approaches, which use (A) the dynamics of the microstates, (B) the qMSM approximation of the generalized master equation, and (C) a hybrid MD/MSM formulation.

2.1 From micro- to macrostate dynamics

In a typical MSM workflow we first construct (say, $n \sim 10^2 - 10^3$) microstates from the MD data, which are subsequently lumped into a few (say, $N \lesssim 10$) macrostates. As explained in the Introduction, we assume that the microstates show Markovian behavior at the chosen lag time τ , which is sufficiently short to resolve the fastest dynamics of interest.

Hence, the microstate transition matrix $\mathbf{t} = \{t_{ij}\}$ satisfies the Chapman-Kolmogorov relation³¹

$$\mathbf{t}(m\tau) = \mathbf{t}^m(\tau), \quad (4)$$

that is, the microstate MSM with lag time τ reproduces correctly the time evolution of the microstate population vector $\mathbf{p}(t) = (p_1, \dots, p_n)^T$. Here the microstate transition matrix $\mathbf{t}(\tau)$ is estimated from the MD data, simply by counting the transitions from state j to state i within lag time τ .

We now combine the above microstates into macrostates $J = 1, \dots, N$ ($N \ll n$), such that each macrostate J contains a specific set of microstates $\{j\}_J$. The macrostate populations $P_J(t)$ are therefore given by

$$P_J(t) = \sum_{j \in J} p_j(t). \quad (5)$$

As for the microstates, we may calculate the corresponding macrostate transition matrix elements $T_{IJ}(\tau)$ from the MD macrostate trajectory by counting the transitions from state J to state I within time τ . Contrary to the microstate MSM, however, the resulting Chapman-Kolmogorov relation for the macrostates is generally not valid, because no clear time separation between intra- and inter-state transitions exists. Hence this ‘local-equilibrium’ approximation of the macrostate transition matrix, $\mathbf{T}_{LE}(\tau)$, cannot correctly reproduce the macrostate populations $P_J(t)$ as found in the MD simulations.

To improve the calculation of the macrostate transition matrix, we follow Hummer and Szabo¹³ and introduce the aggregation matrix $\mathbf{A} \in \mathbb{R}^{n \times N}$ with elements $A_{iJ} = 1$ (if $i \in J$) and $A_{iJ} = 0$ otherwise. This allows us to rewrite Eq. (5) in vectorial notation,

$$\mathbf{P}(t) = \mathbf{A}^T \mathbf{p}(t). \quad (6)$$

To derive a similar relation between the $n \times n$ matrix \mathbf{t} and the $N \times N$ matrix \mathbf{T} , we define the diagonal matrices $\mathbf{D}_n \in \mathbb{R}^{n \times n}$ and $\mathbf{D}_N \in \mathbb{R}^{N \times N}$, whose elements are given by the normalized equilibrium populations $p_i^{\text{eq}} \equiv \pi_i$ and $P_J^{\text{eq}} \equiv \Pi_J$, respectively.¹³ Using \mathbf{D}_N and \mathbf{D}_n to normalize the aggregation matrices \mathbf{A} and \mathbf{A}^T , we find $\mathbf{A}^T \mathbf{D}_n \mathbf{A} \mathbf{D}_N^{-1} = \mathbf{1}_N$, as can be verified by insertion. This leads to the desired relation between micro- and macrostate transition matrices

$$\mathbf{T}(t) = \mathbf{A}^T \mathbf{t}(t) \mathbf{D}_n \mathbf{A} \mathbf{D}_N^{-1}. \quad (7)$$

It can be evaluated in various ways. In the local-equilibrium approximation, we first calculate the microstate transition matrix $\mathbf{t}(\tau)$, perform the transformation to get the corresponding macrostate transition matrix $\mathbf{T}(\tau)$, and arrive at the MSM expression

$$\mathbf{T}_{LE}(m\tau) = \mathbf{T}_{LE}^m(\tau) = \left[\mathbf{A}^T \mathbf{t}(\tau) \mathbf{D}_n \mathbf{A} \mathbf{D}_N^{-1} \right]^m. \quad (8)$$

That is, to evaluate $\mathbf{T}_{LE}^m(\tau)$, in effect we only need the definition of the macrostates.

What is more, Eq. (7) suggest also an alternative and potentially better approximation of $\mathbf{T}(t)$. Since we initially assumed that microstate transition matrix $\mathbf{t}(\tau)$ satisfies the Chapman-Kolmogorov relation in Eq. (4), we may first calculate the microstate time evolution via Eq. (4) and subsequently perform the transformation to the macrostate transition matrix, i.e.

$$\mathbf{T}_{\text{Mic}}(m\tau) = \mathbf{A}^T \mathbf{t}^m(\tau) \mathbf{D}_n \mathbf{A} \mathbf{D}_N^{-1}. \quad (9)$$

This microstate-based evaluation of the macrostate transition matrix preserves all dynamical properties established for the microstates. For example, it yields by design exact macrostate population dynamics, and also provides correct state-to-state waiting times and transition pathways from a microstate Monte Carlo Markov chain simulations with subsequent projection on the macrostates. While the definition of \mathbf{T}_{Mic} is straightforward and its virtues are clearly promising, this microstate-based approach has to the best of our knowledge not yet been mentioned. Compared to the local-equilibrium approximation that yields a constant transition matrix $\mathbf{T}_{\text{LE}}(\tau)$ and the MSM relation (8), however, the microstate-based evaluation results in a time-dependent macrostate transition matrix.

Alternatively, Hummer and Szabo¹³ used a Laplace transformation to derive a long-time approximation of the macrostate transition matrix, which leads to an optimal projection of the microstate dynamics onto the macrostate dynamics. They obtained $\mathbf{T}_{\text{HS}}(m\tau) = \mathbf{T}_{\text{HS}}^m(\tau)$ with

$$\mathbf{T}_{\text{HS}}(\tau) = \mathbf{1}_N + \mathbf{D}_N - \mathbf{D}_N \left[\mathbf{A}^T (\mathbf{1}_n + \mathbf{D}_n - t(\tau))^{-1} \mathbf{D}_n \mathbf{A} \right]^{-1}, \quad (10)$$

which provides a constant transition matrix $\mathbf{T}_{\text{HS}}(\tau)$, but requires the inversion of n - and N -dimensional matrices.

Hence, we have introduced three ways to calculate $\mathbf{T}(m\tau)$ from $\mathbf{t}(\tau)$: The standard local-equilibrium approximation [Eq. (8)], the Hummer-Szabo expression [Eq. (10)], and the microstate-based evaluation [Eq. (9)].

2.2 qMSM evaluation of the generalized master equation

Huang and coworkers¹⁷ recently derived a generalized master equation for the transition matrix $\mathbf{T}(t)$ of the form

$$\dot{\mathbf{T}}(t) = \dot{\mathbf{T}}(0)\mathbf{T}(t) + \int_0^{\min[t, \tau_K]} \mathbf{K}(t') \mathbf{T}(t-t') dt'. \quad (11)$$

Compared to Eq. (3), it contains the additional term $\dot{\mathbf{T}}(0)\mathbf{T}(t)$, which reflects the time evolution of the system without interaction with the environment. Moreover, the upper bound of the integral assumes that the memory kernel $\mathbf{K}(t)$ decays within the (presumably short) time τ_K .

To solve Eq. (11), we discretize the equation by introducing $t = t_n = n\Delta t$, $\mathbf{T}(t_n) = \mathbf{T}_n$ and $\mathbf{K}(t_n) = \mathbf{K}_n$, yielding

$$\dot{\mathbf{T}}_n = \dot{\mathbf{T}}_0 \mathbf{T}_n + \Delta t \sum_{m=1}^n \mathbf{K}_m \mathbf{T}_{n-m}. \quad (12)$$

The main idea of the qMSM approach is to first obtain a short-time approximation of the transition matrix from the MD data, $\mathbf{T} \approx \mathbf{T}_{\text{MD}}$. Subsequently, \mathbf{T}_{MD} is used to iteratively solve Eq. (11) for the memory matrix via

$$\mathbf{K}_n = \frac{\dot{\mathbf{T}}_n - \dot{\mathbf{T}}_0 \mathbf{T}_n}{\Delta t} - \sum_{m=1}^{n-1} \mathbf{K}_m \mathbf{T}_{n-m}. \quad (13)$$

Inserting the resulting \mathbf{K}_n in Eq. (12), we obtain the desired evolution of $\mathbf{T}(t)$ for long times ($t \gg \tau_K$). Hence the qMSM formulation facilitates a straightforward approximate solution of an in principle exact generalized master equation, and also explicitly provides the memory matrix $\mathbf{K}(t)$ that accounts for the non-Markovian dynamics of the system. Requiring only MD data of length $t \approx \tau_K$, qMSM allows us to predict long-time dynamics from short trajectories. The

above equations were implemented in an in-house Python code following Ref. 32; the kernel decay time τ_K was obtained either directly from the memory kernel (in the one-dimensional toy model), or via the mean integral memory kernel¹⁷ (for HP35).

While the qMSM inversion scheme [i.e., solving Eq. (13) to get \mathbf{K} and inserting it in Eq. (12) to get \mathbf{T}] appears to be a straightforward data-driven approach to parameterize the generalized master equation, there are several peculiarities of the qMSM method. For one, we note that –given long enough MD data– the MD-based matrix \mathbf{T}_{MD} is the best transition matrix you can get. Hence, by calculating \mathbf{K} from \mathbf{T}_{MD} via Eq. (13) and inserting it in Eq. (12), the resulting transition matrix \mathbf{T} can only be worse than the initial matrix \mathbf{T}_{MD} . Iterating the procedure [by using the new \mathbf{T} to again calculate \mathbf{K} and then again \mathbf{T}] does not help either, because we obtain the same result as in the first iteration (as readily shown by insertion).

Another issue is that qMSM keeps the additional term $\dot{\mathbf{T}}(0)\mathbf{T}(t)$, which typically vanishes for symmetry reasons,¹⁶ but may be non-zero in a numerical evaluation. Interestingly, this term exactly cancels the memory kernel at $t = 0$ [which can be shown by calculating \mathbf{T}_n and \mathbf{K}_n for $n = 0$ from Eqs. (12) and (13), respectively]. While this is again a consequence of the chosen discretization, it seems odd, because \mathbf{K}_0 is the only non-zero term in the Markov limit. In all cases considered, however, the neglect of the term seems to hardly change the numerical results. Another practical issue is that the calculation of the memory matrix from Eq. (13) can be seriously plagued by noise resulting from the MD data and the time derivatives. As a remedy, recently an integrative ansatz²⁵ and a time-convolutionless approach²⁰ of the generalized master equation were proposed.

2.3 Hybrid MD/MSM formulation

In the Introduction, we opposed in Eqs. (1) and (2) two standard ways to estimate the macrostate transition matrix $\mathbf{T}(t) = \{\mathbf{T}_{IJ}(t)\}$. On the one hand, we may use the MD data to directly count the transitions from state J to state I within time t . The resulting transition matrix $\mathbf{T}_{\text{MD}}(t)$ generates the correct time evolution of the state model according to Eq. (1), but is limited to times $t \approx t_{\text{max}}$ with t_{max} being the length of the MD trajectories (and actually even some hundreds MD frames less to facilitate a sufficient time average). On the other hand, we may invoke the Markov approximation to obtain $\mathbf{T}(t = m\tau) \approx \mathbf{T}^m(\tau)$, which assumes that the transition matrix $\mathbf{T}(t)$ becomes constant for $t \gtrsim \tau$. While this only requires short MD trajectories, we need to choose a lag time τ that is long enough to achieve Markovianity, but at the same time short enough to resolve the fastest dynamics of interest.

To have the best of both worlds, we may simply combine the two approaches by using $\mathbf{T}_{\text{MD}}(t)$ at short times and employing some formulation (including local equilibrium, Hummer-Szabo, or microstate-based) to construct a MSM using the long lag time t_{max} , i.e.,

$$\mathbf{T}_{\text{MD/MSM}}(t) = \begin{cases} \mathbf{T}_{\text{MD}}(t) & t \leq t_{\text{max}}, \\ \mathbf{T}_{\text{MSM}}^m(t_{\text{max}}) & t = mt_{\text{max}}. \end{cases} \quad (14)$$

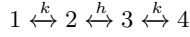
In this way, we use at short times the approximation-free transition matrix $\mathbf{T}_{\text{MD}}(t)$, including full time resolution (as given by the MD data). At long times, the MSM typically can use a rather long lag time.

3 Results

To compare the performance of the different methods, we test them on two model systems: A one-dimensional toy model lumping four microstates into two macrostates, and a recently established³³ benchmark MSM of the folding of villin headpiece (aka HP35) using a long MD trajectory by Piana et al.³⁰

3.1 One-dimensional toy model

As a simple instructive model, Fig. 1a shows the free energy landscape of a system with four microstates i ($i = 1, \dots, 4$), which are lumped into two macrostates I ($I = L, R$ for left and right state). Following Hummer and Szabo,¹³ we define the model via its microstate transitions



with transition probabilities k and h . The resulting microstate transition matrix reads

$$\mathbf{t} = \begin{bmatrix} 1-k & k & 0 & 0 \\ k & 1-(k+h) & h & 0 \\ 0 & h & 1-(h+k) & k \\ 0 & 0 & k & 1-k \end{bmatrix}. \quad (15)$$

Because \mathbf{t} is symmetric and detailed balance holds ($t_{ij}\pi_j = t_{ji}\pi_i$), the microstate equilibrium populations are $\pi_i = 1/4$. The eigenvalues of the matrix are $\lambda_0 = 1$, $\lambda_1 = 1 - h - k + \sqrt{h^2 + k^2}$, $\lambda_2 = 1 - 2k$, and $\lambda_3 = 1 - h - k - \sqrt{h^2 + k^2}$. Hence, the longest (nontrivial) microstate implied timescale is

$$t_{\text{micro}} \equiv t_1/\tau_0 = -\frac{1}{\ln \lambda_1} = -\frac{1}{\ln(1 - h - k + \sqrt{h^2 + k^2})}, \quad (16)$$

where we introduced the unit time τ_0 to define a dimensionless time t_{micro} .

When we combine microstates 1 and 2 into macrostate L and microstates 3 and 4 into macrostate R , the probability k accounts for intrastate transitions (i.e., within L or R) and h accounts for interstate transitions (i.e., between L and R) of the macrostate model, see Fig. 1a. We study the model both in the case of good lumping (i.e., a sufficient timescales separation between fast intrastate and slow interstate motions) and in the case of bad lumping. The latter means that we have a low energy barrier between macrostates L and R , and high barriers between microstates that belong to the same macrostate. This leads to a bad timescales separation, causing the model to behave non-Markovian.

Due to the simplicity of the model, we can derive analytical expressions for the 2×2 macrostate transition matrix. In the local equilibrium approximation [Eq. (8)], we obtain

$$\mathbf{T}_{\text{LE}}(t = m\tau_0) = \begin{bmatrix} 1 - h/2 & h/2 \\ h/2 & 1 - h/2 \end{bmatrix}^m. \quad (17)$$

Notably, \mathbf{T}_{LE} does not depend on the intrastate transition rate k , as it is assumed to be much higher than any other timescale of the macrostate model. The single (nontrivial) macrostate implied timescale is

$$t_{\text{LE}} = -\frac{1}{\ln(1 - h)}. \quad (18)$$

The Hummer-Szabo projection [Eq. (10)] gives $\mathbf{T}_{\text{HS}}(t =$

$m\tau_0) = \mathbf{T}_{\text{HS}}^m$ with¹³

$$\mathbf{T}_{\text{HS}} = \mathbf{1}_2 + \frac{hk}{h + 2k} \begin{bmatrix} -1 & 1 \\ 1 & -1 \end{bmatrix}, \quad (19)$$

which takes into account both intra- and inter-state transitions. The resulting implied timescale is

$$t_{\text{HS}} = -\frac{1}{\ln\left(1 - \frac{2hk}{h+2k}\right)}. \quad (20)$$

In the microstate-based approach [Eq. (9)] and the qMSM method [Eq. (12)], the transition matrices $\mathbf{T}_{\text{Mic}}(t)$ and $\mathbf{T}_{\text{qMSM}}(t)$ are calculated numerically, because no simple analytical expressions exist. Note that the implied timescales of $\mathbf{T}_{\text{Mic}}(t)$ and $\mathbf{T}_{\text{qMSM}}(t)$ depend on time, while the implied timescales t_{micro} , t_{LE} , and t_{HS} are constant.

As a first test, we wish to study how the various formulations reproduce the reference implied timescale t_{micro} of the microstates. Choosing $k = h = 0.1$ (weakly non-Markovian case), Fig. 1b shows that the local equilibrium approximation t_{LE} underestimates t_{micro} almost by a factor 2, while the Hummer-Szabo result is only shorter by 13%. The results obtained for $\mathbf{T}_{\text{Mic}}(t)$ and $\mathbf{T}_{\text{qMSM}}(t)$ reveal that the microstate-based method converges to the correct result and that qMSM converges to a value that is 9% shorter than t_{micro} . (In all cases, we choose the qMSM kernel decay time τ_K such that the normalized memory kernel satisfies $K(\tau_K) \leq 0.1$.) To compare to a largely Markovian case ($h/k = 0.2$), Fig. S1 shows that all methods yield the correct timescale t_{micro} , except for the local equilibrium approximation, which gives $t_{\text{LE}} = 0.9 t_{\text{micro}}$.

We now choose $t = 100$ (where qMSM and microstate-based results are virtually constant), and vary the Markovianity parameter h/k from $h/k \ll 1$ (Markovian case) to $h/k \gtrsim 1$ (non-Markovian case). While for $h = 0.1$, $k = 0.5$ all methods yield the correct microstate timescale t_{micro} (except for t_{LE}), the results vary considerably in the non-Markovian case. Choosing $h = 0.5$, $k = 0.1$, for example, t_{LE} underestimates t_{micro} by 87%, t_{HS} by 40%, and t_{qMSM} by 27%, while the microstate-based result closely matches the reference.

We now consider the quality of the underlying time-dependent transition matrices. As the diagonal elements $T_{II}(t)$ ($I = L, R$) represent the state populations $P_L(t) = 1 - P_R(t)$, which also determine the off-diagonal elements $T_{LR} = 1 - P_L$ and $T_{RL} = 1 - P_R$, it is sufficient to focus on $P_L(t) \equiv P(t)$. By design, $P(0) = 1$ and $P(\infty) = \Pi_L = 0.5$, such that the various formulations only differ by the rate of the decay. Because the microstates produce the exact dynamics of the model, the microstate-based calculation $P_{\text{Mic}}(t)$ coincides with this reference.

Choosing $h/k = 1$ and $h/k = 5$, Figs. 1d and 1e compare the population $P(t)$ obtained from the various formulations. While for $h/k = 1$ all methods are quite close to the reference results, we find significant deviations in the strongly non-Markovian case $h/k = 5$, where $P(t)$ in fact reveals two timescales. That is, the population exhibits a strong initial decay to $P(1) = 0.75$ during the first time step, reflecting fast transitions over the shallow barrier at $x = 0$ (Fig. 1a). All formulations reproduce this value correctly, except for the long-time approximation $P_{\text{HS}}(t)$, which coincides with the reference for $t \gtrsim 7$. Being a short-time approximation, $P_{\text{LE}}(t)$ decays significantly too fast for $t > 1$. The qMSM calculation represents a clear improvement over these ap-

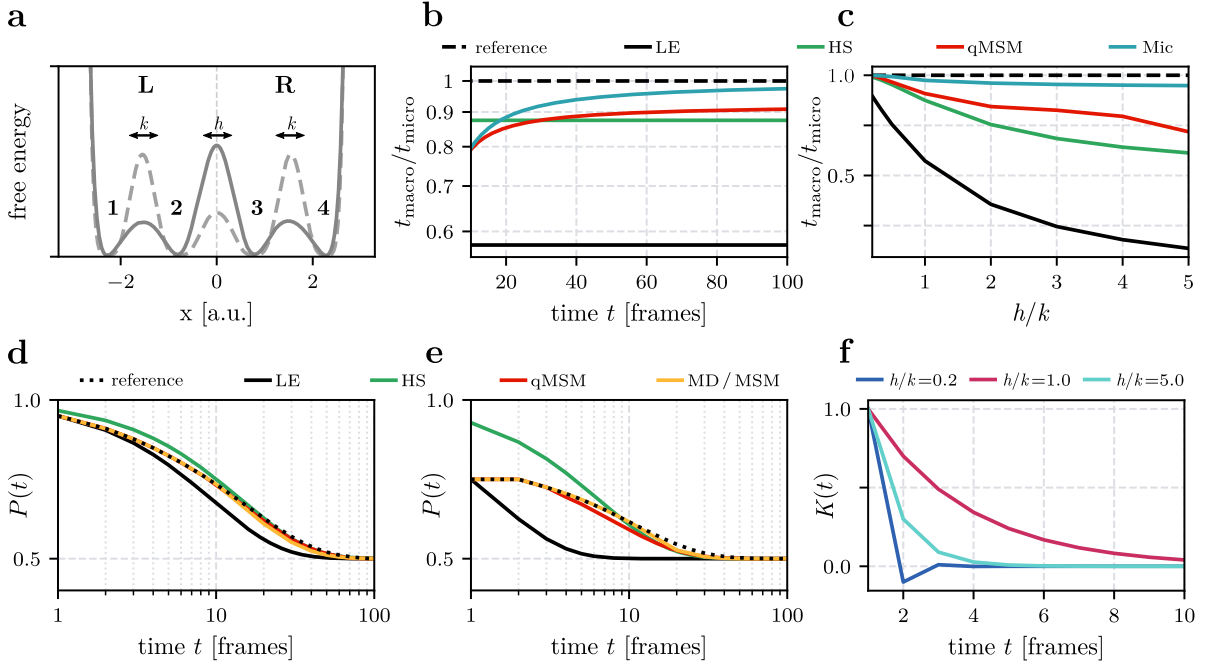


Figure 1: One-dimensional toy model. (a) Schematic free energy landscape, indicating four microstates 1, 2, 3 and 4, which are lumped into two macrostates L and R . Depending on the ratio of the interstate transition probability h and the intrastate transition probability k , the macrostate dynamics is Markovian ($h/k \ll 1$, dark gray) or non-Markovian ($h/k \gtrsim 1$, dashed). (b) Ratio of the macroscopic and microscopic implied timescales $t_{\text{macro}}/t_{\text{micro}}$ of the two-macrostate model for $h/k = 1$. Compared are the reference result obtained from the microstates (dashed black), the local equilibrium approximation (black), and the Hummer-Szabo projection (green), as well as the time evolution the result from qMSM (red) and of the microstate-based result (blue). (c) Normalized implied timescales obtained from the various methods, drawn as a function of the Markovianity parameter h/k . Time evolution of the macrostate population of the various methods, shown for (d) $h/k = 1$ and (e) $h/k = 5$. Also shown are results of the hybrid MD/MSM calculation [Eq. (14)] with $t_{\text{max}} = 10$. (f) Normalized memory kernel $K(t)$ of the qMSM method, obtained for $h/k = 0.2$ (blue), $h/k = 1$ (red), and $h/k = 5$ (green).

proximations and reproduces the exact results closely. Finally, we also show the hybrid calculation [Eq. (14)], which uses until $t_{\text{max}} = 10$ the exact transition matrix $\mathbf{T}_{\text{MD}}(t)$, and for longer times the local approximation $\mathbf{T}_{\text{LE}}(t = mt_{\text{max}})$. For this choice of t_{max} , the hybrid result virtually matches the reference at all times.

Unlike the other methods, the generalized master equation (11) underlying the qMSM method involves the calculation of a memory matrix $\mathbf{K}(t)$, which reports on the non-Markovianity of the dynamics. Since for symmetry reasons $K_{LL} = K_{RR} = -K_{LR} = -K_{RL}$, it is sufficient to focus on $K_{LL}(t)$. Considering the cases $h/k = 0.2, 1$, and 5 , Fig. 1f shows the normalized memory kernel $K(t) = K_{LL}(t)/K_{LL}(1)$. As expected, in the Markovian limit ($h/k = 0.2$) the memory decays essentially within a single time step. Less expected, though, we find that the slowest decay (~ 2.8) is obtained for weakly non-Markovian case ($h/k = 1$), while in the strongly non-Markovian case ($h/k = 5$), the decay (~ 0.8) is again faster, although clearly slower than the Markovian case.

To explain this finding, we recall that the memory kernel $K(t)$ is meant to reflect the intrastate dynamics of the macrostates, which in turn depends on the implied timescales t_k ($k = 1, 2, 3$) and associated eigenvectors of the microstate MSM. As shown in Tab. S1, the first timescale and eigenvector clearly indicate transitions between the left states ($L = 1, 2$) and the right states ($R = 3, 4$), while the second and third eigenvectors reflect transitions within L and R . In the Markovian limit ($h/k = 0.2$), we find $t_2 = 0.45$ and $t_3 = 0.26$, which indeed coincide with the decay of the memory kernel $K(t)$ in Fig. 1d. Moreover, for $h/k = 1$, we

obtain $t_2 = 4.5$ and $t_3 = 2.4$, which again are similar to the decay time (~ 2.8) of $K(t)$. In the strongly non-Markovian case ($h/k = 5$), however, this coincidence is less clear, as we get $t_2 = 4.5$ and $t_3 = 0.45$, but a memory decay time of 0.8 . Interestingly, we also find that for $h/k = 5$ the amplitude $K(1)$ of the memory is about twenty times larger than in the first two cases. These findings indicate that the interpretation of the qMSM memory kernel in terms of memory timescales is generally not straightforward.³⁴

3.2 The folding of HP35

To learn how the above findings for the toy model generalize to the case of all-atom MD data, we now consider the folding of villin headpiece (HP35) as a well-established model problem. As in previous work,^{33,35} we use a $\sim 300\mu\text{s}$ -long MD trajectory of the fast folding Lys24Nle/Lys29Nle mutant of HP35 at $T = 360\text{ K}$ by Piana et al.,³⁰ which shows about 30 folding events. Following the benchmark study of Nagel et al.,³³ we employ the following MSM workflow. Firstly, we use MoSAIC correlation analysis³⁶ to perform a feature selection resulting in 42 contact distances. Next, we eliminate high-frequency fluctuations of the distance trajectory, by employing a Gaussian low-pass filter³⁵ with a standard deviation of $\sigma = 2\text{ ns}$. Employing principal component analysis on these contacts,³⁷ we use the resulting first five components for subsequent robust density based clustering³⁸ into 547 microstates. In a final step, we adopt the most probable path algorithm³⁹ to dynamically lump the microstates into 12 metastable macrostates, using a lag time of 10 ns . The resulting dynamical model compares favorably

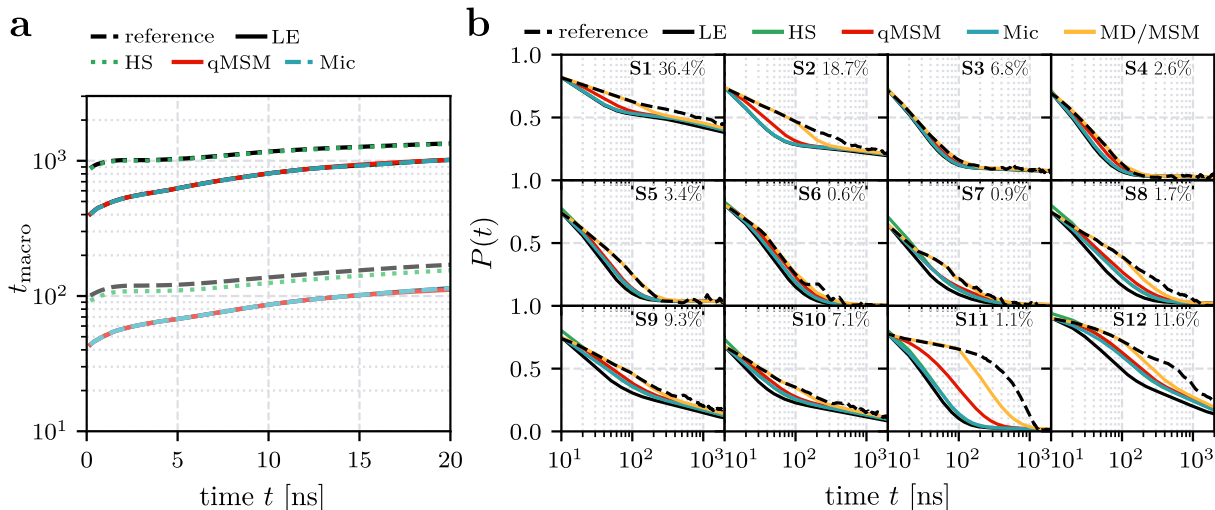


Figure 2: Twelve-state MSM constructed from a $300\mu\text{s}$ -long MD trajectory³⁰ of the folding of HP35. (a) First two implied timescales obtained from the microstates (dashed black, reference), the local equilibrium approximation (using the lag time $\tau = 10$ ns, black), the Hummer-Szabo projection (using $\tau = 10$ ns, green), the microstate-based result (blue), and the result from qMSM (using the kernel time $\tau_K = 10$ ns, red). (b) Chapman-Kolmogorov test of the twelve macrostates, comparing the reference MD state trajectory to the various versions of the theory. Also shown are results of the hybrid MD/MSM calculation [Eq. (14)] with $t_{\text{max}} = 100$ ns.

to MSMs from alternative combinations of methods³³ and explains the folding of HP35 as cooperative transition between folded and unfolded energy basins and several intermediate states. In this work, we employ the partitioning of the MD trajectory into micro- and macrostates, in order to calculate the various versions of the macrostate transition matrix introduced above.

We begin with the discussion of the first two implied timescales, which are depicted in Fig. 2a as a function of the lag time. As discussed in Ref. 33, the slowest timescale ($\sim 1.5\mu\text{s}$) corresponds to the overall folding process, while the next two timescales ($\sim 0.1\mu\text{s}$) account for conformational rearrangement in the native and the unfolded basins. Taking again the microstate timescales as a reference, we overall find the Hummer-Szabo results being in excellent agreement, followed by the results from the local equilibrium approximation, which virtually coincide with the qMSM and the microstate-based results.

As most important assessment, Fig. 2b shows the Chapman-Kolmogorov test of the twelve macrostates, which compare the macrostate projection of the MD trajectory (providing the reference) to the various versions of the theory. As a result of a careful selection of features and methods, the benchmark model³³ represents a valuable MSM. Consequently, the deviations of the various methods are overall only minor, and already the simple local equilibrium approximation matches the correct population dynamics of most macrostates quite closely. Quite similar is the Hummer-Szabo projection, despite its superior modeling of the implied timescales above.

Recalling that the microstate-based calculation should coincide with the reference MD results in the case of a truly Markovian partitioning of the microstates, we learn that the microstates are a main reason for the deviations of the Chapman-Kolmogorov tests. Not relying on the quality of the microstates, the qMSM in fact represents an improvement of the microstate-based methods, particularly in the case of ill-defined states such as states 2 and 11. (Judging from the time evolution of the qMSM memory matrix $\mathbf{K}(t)$ shown in Fig. S2, we chose $\tau_K = 10$ ns where, apart from

residual fluctuations around zero, all elements $K_{IJ}(t)$ are safely decayed.) Even better is the performance of a hybrid calculation [Eq. (14)], which uses until $t_{\text{max}} = 100$ ns the exact transition matrix $\mathbf{T}_{\text{MD}}(t)$, and for longer times the local approximation $\mathbf{T}_{\text{LE}}(t = mt_{\text{max}})$. Apart from the ill-defined states 2 and 11, the hybrid calculation matches the reference very accurately.

While a single, long MD trajectory is certainly perfect for building an MSM, in practice we often have many short trajectories (since they are readily computed in parallel). In principle, trajectories as short as the lag time τ and the kernel time τ_K should be already sufficient to construct an MSM and a qMSM, respectively. However, the validity of this presumption has been rarely assessed due to the lack of long reference trajectories. As we used $\tau = \tau_K = 10$ ns in the calculations above, and we need some extra time for the time averages to calculate transition probabilities, we decided to split the $300\mu\text{s}$ trajectory in 10000×30 ns (150 frames) long pieces, such that we can average over 100 frames. Note that 30 ns is quite short considering the overall folding time of $\sim 2\mu\text{s}$ of HP35. As the MSM workflow explained above employs no time information up to the density based clustering included,⁴⁰ we can use the same microstates. On the other hand, the dynamical lumping of these states via the most probable path algorithm³⁹ requires calculations based on the transition matrix, which differs in the case of one long and of many short trajectories. Hence, the resulting macrostates differ minor from the ones obtained from the single $300\mu\text{s}$ trajectory, see Fig. S3. Lastly, we again calculated the macrostate transition matrices for the various theoretical formulations.

Figure 3 shows the implied timescales and Chapman-Kolmogorov tests of the resulting MSMs. Overall the short-trajectories results look very similar to the results from the single long trajectory (Fig. 2), thus confirming the promise of MSMs to describe long-time dynamics from short trajectories. However, it should be kept in mind that these short trajectories used adequately chosen initial conditions, because they were taken from a long trajectory that exhibits numerous folding and unfolding transition. This is less ob-

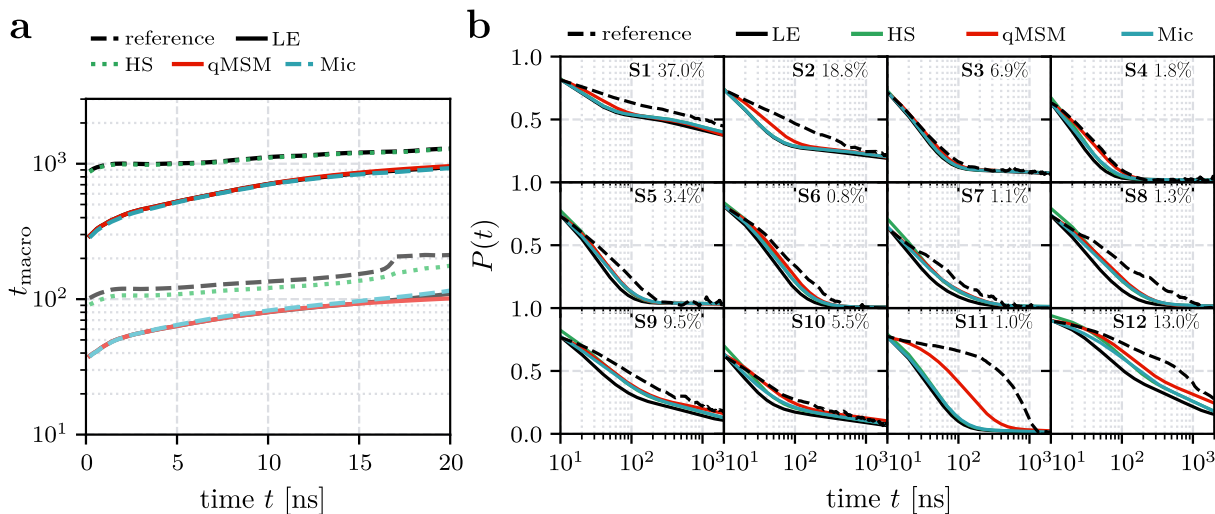


Figure 3: As in Fig. 2, except that the original $300\mu\text{s}$ -long trajectory of HP35 was split in $10\,000 \times 30\text{ ns}$ trajectories. The hybrid MD/MSM method is not shown, as for $t_{\text{max}} = 10\text{ ns}$ it coincides with the local equilibrium approximation.

vious without such a reactive trajectory, although various strategies have been proposed to obtain good initial conditions along the reaction paths of a considered process.^{41–43}

4 Concluding remarks

We have outlined the theoretical basis of various approaches to estimate the macrostate transition matrix of an MSM, from the standard local equilibrium approximation to a sophisticated generalized master equation approach. Employing a one-dimensional toy model and an all-atom folding trajectory of HP35, we have provided a comprehensive comparison of the various formulations, and introduced two new methods, the microstate-based approach in Eq. (9) and the hybrid MD/MSM ansatz in Eq. (14).

The most commonly used method, the local equilibrium approximation [Eq. (8)], simply counts the transitions between the macrostates within a certain lag time, which assumes Markovian data with a timescale separation between fast intrastate fluctuations and slow interstate transitions. As shown for the toy model in Fig. 1, which allows to tune the ratio between these timescales, the quality of the resulting implied timescale and the Chapman-Kolmogorov test readily deteriorate, when this separation is not fulfilled.

Assuming that Markovianity is at least given at the microstate level, the knowledge of the microstate dynamics can be exploited to construct improved macrostate dynamics. For one, this is used in the Laplace transform-based method by Hummer and Szabo,¹³ which was shown to achieve significantly improved Markovianity in all considered cases. However, we can also directly employ a microstate-to-macrostate projection to construct a macrostate transition matrix $\mathbf{T}_{\text{Mic}}(t)$ [Eq. (9)], which by design yields correct macrostate population dynamics. As an important consequence, this means that residual non-Markovian behavior of the resulting MSM must be caused by sub-optimal microstates (and not by the lumping of micro-into macrostates). By performing microstate Monte Carlo Markov chain simulations with subsequent projection on macrostates, this new and promising microstate-based approach may also provide state-to-state waiting times and transition pathways.

Not relying on the quality of the microstates, generalized

master equations, such as the qMSM ansatz of Huang and coworkers¹⁷ provide an alternative approach to deal with non-Markovian dynamics. In fact, we found that qMSM performs well even in the case of ill-defined macrostates of HP35 (Fig. 2) and in the case of short-trajectory data (Fig. 3). We discussed several peculiarities of the approach, including the interpretation of the memory kernel matrix and its calculation from noisy data.

In practice, an MSM is often used to interpret given MD data in terms of the time evolution of the populations $P_I(t)$ of metastable conformational states. For the length of the MD trajectories t_{max} (actually some hundreds MD frames less to facilitate a sufficient time average), we can simply project the MD data on these states, without invoking a dynamical approximation such as the assumption of Markovianity. In the ‘hybrid MD/MSM’ method [Eq. (14)], we exploit this idea to obtain the system’s short time evolution with good time resolution, and subsequently use some formulation (including local equilibrium, Hummer-Szabo, or microstate-based) to construct a MSM using the long lag time t_{max} . Given sufficiently long trajectories, this strategy of combining the best of two worlds is simple and promises prime results. While the definition of the hybrid MD/MSM method and its virtues seem obvious, it has to the best of our knowledge not yet been fully appreciated.

Acknowledgments

The authors thank Georg Diez, Daniel Nagel and Tim Uttenweiler for helpful comments and discussions, as well as D. E. Shaw Research for sharing their trajectories of HP35. This work has been supported by the Deutsche Forschungsgemeinschaft (DFG) within the framework of the Research Unit FOR 5099 ‘Reducing complexity of nonequilibrium’ (project No. 431945604), the High Performance and Cloud Computing Group at the Zentrum für Datenverarbeitung of the University of Tübingen and the Rechenzentrum of the University of Freiburg, the state of Baden-Württemberg through bwHPC and the DFG through Grant Nos. INST 37/935-1 FUGG (RV bw16I016) and INST 39/963-1 FUGG (RV bw18A004), the Black Forest Grid Initiative, and the Freiburg Institute for Advanced Studies (FRIAS) of the Albert-Ludwigs-University Freiburg.

Data Availability Statement

The simulation data and all intermediate results for our reference model of HP35, including detailed descriptions to reproduce all steps of the analyses, can be downloaded from <https://github.com/moldyn/HP35>.

Supporting Information Available

Includes a table comprising the eigenvectors, timescales, and kernel decay times of all considered one-dimensional models, as well as figures of the time evolution of the memory kernel of HP35, and of the structural characterization of the states of the short-trajectory MSM of HP35.

References

- (1) Berendsen, H. J. C. *Simulating the Physical World*; Cambridge University Press: Cambridge, 2007.
- (2) Lange, O. F.; Grubmüller, H. Collective Langevin dynamics of conformational motions in proteins. *J. Chem. Phys.* **2006**, *124*, 214903.
- (3) Hegger, R.; Stock, G. Multidimensional Langevin modeling of biomolecular dynamics. *J. Chem. Phys.* **2009**, *130*, 034106.
- (4) Ayaz, C.; Tepper, L.; Brüning, F. N. et al. Non-Markovian modeling of protein folding. *Proc. Natl. Acad. Sci. USA* **2021**, *118*, e2023856118.
- (5) Buchete, N.-V.; Hummer, G. Coarse master equations for peptide folding dynamics. *J. Phys. Chem. B* **2008**, *112*, 6057–6069.
- (6) Bowman, G. R.; Beauchamp, K. A.; Boxer, G. et al. Progress and challenges in the automated construction of Markov state models for full protein systems. *J. Chem. Phys.* **2009**, *131*, 124101.
- (7) Prinz, J.-H.; Wu, H.; Sarich, M. et al. Markov models of molecular kinetics: generation and validation. *J. Chem. Phys.* **2011**, *134*, 174105.
- (8) Bowman, G. R.; Pande, V. S.; Noé, F. *An Introduction to Markov State Models*; Springer: Heidelberg, 2013.
- (9) Scherer, M. K.; Trendelkamp-Schroer, B.; Paul, F. et al. PyEMMA 2: A Software Package for Estimation, Validation, and Analysis of Markov Models. *J. Chem. Theory Comput.* **2015**, *11*, 5525–5542.
- (10) Beauchamp, K. A.; Bowman, G. R.; Lane, T. J. et al. MSM-Builder2: Modeling Conformational Dynamics on the Picosecond to Millisecond Scale. *J. Chem. Theory Comput.* **2011**, *7*, 3412–3419.
- (11) Nagel, D.; Stock, G. msmhelper: A Python package for Markov state modeling of protein dynamics. *J. Open Source Softw.* **2023**, *8*, 5339.
- (12) Röblitz, S.; Weber, M. Fuzzy spectral clustering by PCCA+: application to Markov state models and data classification. *Adv. Data Anal. Classif.* **2013**, *7*, 147–179.
- (13) Hummer, G.; Szabo, A. Optimal Dimensionality Reduction of Multistate Kinetic and Markov-State Models. *J. Phys. Chem. B* **2015**, *119*, 9029–9037.
- (14) Kells, A.; Mihalka, Z. E.; Annibale, A. et al. Mean first passage times in variational coarse graining using Markov state models. *J. Chem. Phys.* **2019**, *150*, 134107.
- (15) Sharpe, D. J.; Wales, D. J. Nearly reducible finite Markov chains: Theory and algorithms. *J. Chem. Phys.* **2021**, *155*, 140901.
- (16) Zwanzig, R. From classical dynamics to continuous time random walks. *J. Stat. Phys.* **1983**, *30*, 255–262.
- (17) Cao, S.; Montoya-Castillo, A.; Wang, W. et al. On the advantages of exploiting memory in Markov state models for biomolecular dynamics. *J. Chem. Phys.* **2020**, *153*, 014105.
- (18) Hartich, D.; Godec, A. Emergent Memory and Kinetic Hysteresis in Strongly Driven Networks. *Phys. Rev. X* **2021**, *11*, 041047.
- (19) Suarez, E.; Wiewiora, R. P.; Wehmeyer, C. et al. What Markov State Models Can and Cannot Do: Correlation versus Path-Based Observables in Protein-Folding Models. *J. Chem. Theory Comput.* **2021**, *17*, 3119–3133.
- (20) Dominic, A. J.; Sayer, T.; Cao, S. et al. Building insightful, memory-enriched models to capture long-time biochemical processes from short-time simulations. *Proc. Natl. Acad. Sci. USA* **2023**, *120*, e2221048120.
- (21) Jung, G.; Hanke, M.; Schmid, F. Iterative Reconstruction of Memory Kernels. *J. Chem. Theory Comput.* **2017**, *13*, 2481–2488.
- (22) Kowalik, B.; Daldrop, J. O.; Kappler, J. et al. Memory-kernel extraction for different molecular solutes in solvents of varying viscosity in confinement. *Phys. Rev. E* **2019**, *100*, 012126.
- (23) Meyer, H.; Wolf, S.; Stock, G. et al. A numerical procedure to evaluate memory effects in non-equilibrium coarse-grained models. *Adv. Theory Simul.* **2020**, *111*, 2000197.
- (24) Unarta, I. C.; Cao, S.; Kubo, S. et al. Role of bacterial RNA polymerase gate opening dynamics in DNA loading and antibiotics inhibition elucidated by quasi-Markov State Model. *Proc. Natl. Acad. Sci. USA* **2021**, *118*, e2024324118.
- (25) Cao, S.; Qiu, Y.; Kalin, M. L. et al. Integrative generalized master equation: A method to study long-timescale biomolecular dynamics via the integrals of memory kernels. *J. Chem. Phys.* **2023**, *159*, 134106.
- (26) Schütte, C.; Noé, F.; Lu, J. et al. Markov state models based on milestoning. *J. Chem. Phys.* **2011**, *134*, 204105.
- (27) Lemke, O.; Keller, B. G. Density-based cluster algorithms for the identification of core sets. *J. Chem. Phys.* **2016**, *145*, 164104.
- (28) Jain, A.; Stock, G. Hierarchical folding free energy landscape of HP35 revealed by most probable path clustering. *J. Phys. Chem. B* **2014**, *118*, 7750–7760.
- (29) Nagel, D.; Weber, A.; Lickert, B. et al. Dynamical coring of Markov state models. *J. Chem. Phys.* **2019**, *150*, 094111.
- (30) Piana, S.; Lindorff-Larsen, K.; Shaw, D. E. Protein folding kinetics and thermodynamics from atomistic simulation. *Proc. Natl. Acad. Sci. USA* **2012**, *109*, 17845–17850.
- (31) We note that Markovianity is a sufficient condition for validity of the Chapman-Kolmogorov equation, not a necessary one. See the discussion in Refs. 34,44 .
- (32) Wu, Y.; Cao, S.; Qiu, Y. et al. Tutorial on how to build non-Markovian dynamic models from molecular dynamics simulations for studying protein conformational changes. *The Journal of Chemical Physics* **2024**, *160*, 121501.
- (33) Nagel, D.; Sartore, S.; Stock, G. Toward a Benchmark for Markov State Models: The Folding of HP35. *J. Phys. Chem. Lett.* **2023**, *14*, 6956–6967.
- (34) Vollmar, L.; Bebon, R.; Schimpf, J. et al. Model-free inference of memory in conformational dynamics of a multi-domain protein. *J. Phys. A: Math. Theor.* **2024**, *57*, 365001.
- (35) Nagel, D.; Sartore, S.; Stock, G. Selecting Features for Markov Modeling: A Case Study on HP35. *J. Chem. Theory Comput.* **2023**, *19*, 3391–3405.
- (36) Diez, G.; Nagel, D.; Stock, G. Correlation-based feature selection to identify functional dynamics in proteins. *J. Chem. Theory Comput.* **2022**, *18*, 5079–5088.
- (37) Ernst, M.; Sittel, F.; Stock, G. Contact- and distance-based principal component analysis of protein dynamics. *J. Chem. Phys.* **2015**, *143*, 244114.
- (38) Sittel, F.; Stock, G. Robust Density-Based Clustering to Identify Metastable Conformational States of Proteins. *J. Chem. Theory Comput.* **2016**, *12*, 2426–2435.
- (39) Jain, A.; Stock, G. Identifying metastable states of folding proteins. *J. Chem. Theory Comput.* **2012**, *8*, 3810–3819.
- (40) As mentioned, we use a Gaussian low-pass filter ($\sigma = 2$ ns) to smooth the input coordinates, which may cause deviations at the beginning and the end of the short trajectories, compared to a filtering of the entire trajectory. As this effect turned out rather small, though, we ignored this effect and used the same microstates for better comparability.
- (41) Bowman, G. R.; Ensign, D. L.; Pande, V. S. Enhanced modeling via network theory: Adaptive sampling of Markov state models. *J. Chem. Theory Comput.* **2010**, *6*, 787–794.
- (42) Biswas, M.; Lickert, B.; Stock, G. Metadynamics Enhanced Markov Modeling: Protein Dynamics from Short Trajectories. *J. Phys. Chem. B* **2018**, *122*, 5508–5514.
- (43) Wan, H.; Voelz, V. A. Adaptive Markov state model estimation using short reseeding trajectories. *J. Chem. Phys.* **2020**, *152*, 024103.

- (44) Lapolla, A.; Godec, A. Toolbox for quantifying memory in dynamics along reaction coordinates. *Phys. Rev. Res.* **2021**, *3*, L022018.

Supporting Information: Markov-type state models to describe non-Markovian dynamics

Sofia Sartore, Franziska Teichmann, and Gerhard Stock*

Biomolecular Dynamics, Institute of Physics, University of Freiburg, 79104 Freiburg, Germany

E-mail: stock@physik.uni-freiburg.de

arXiv:2412.08660v2 [cond-mat.soft] 16 Jan 2025

Table S1: Timescales of the 4-state toy model, obtained for the three cases with different Markovianity. Shown are the three implied timescales t_k , the corresponding eigenvectors, the decay time of the memory kernel τ_k , and the initial values of the memory kernel $K(1)$.

	$\mathbf{h} = 0.1, \mathbf{k} = 0.5$	$\mathbf{k} = 0.1 = \mathbf{h}$	$\mathbf{h} = 0.5, \mathbf{k} = 0.1$
t_1	10.6	16.6	10.59
t_2	0.45	4.48	4.48
t_3	0.26	2.39	0.45
eigenvectors			
τ_k	0.45	2.8	0.83
$K(1)$	0.005	0.005	0.12

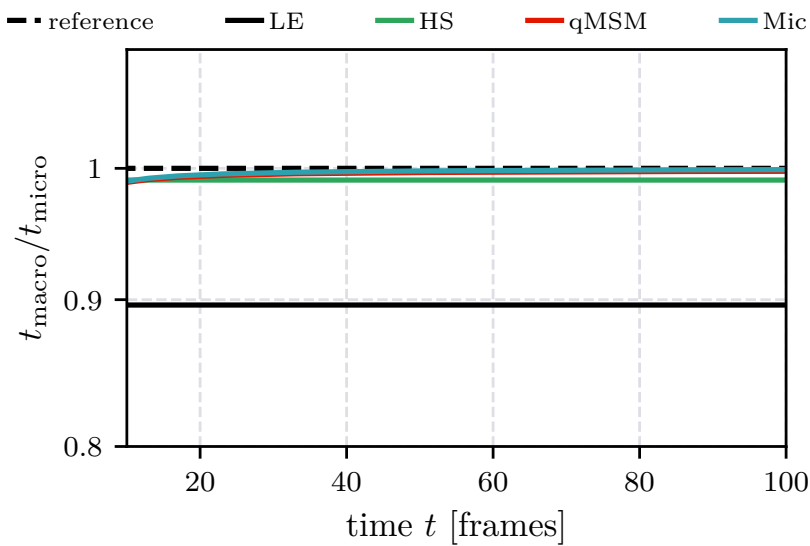


Figure S1: Implied timescale t_{macro} of the two-macrostate toy model for the Markovian case $h/k = 0.2$. Compared are the reference result obtained from the microstates (dashed black), the local equilibrium approximation (black), and the Hummer-Szabo projection (green), as well as the time evolution the result from qMSM (using the Kernel time $\tau_K = 3$, red) and of the microstate-based result (blue).

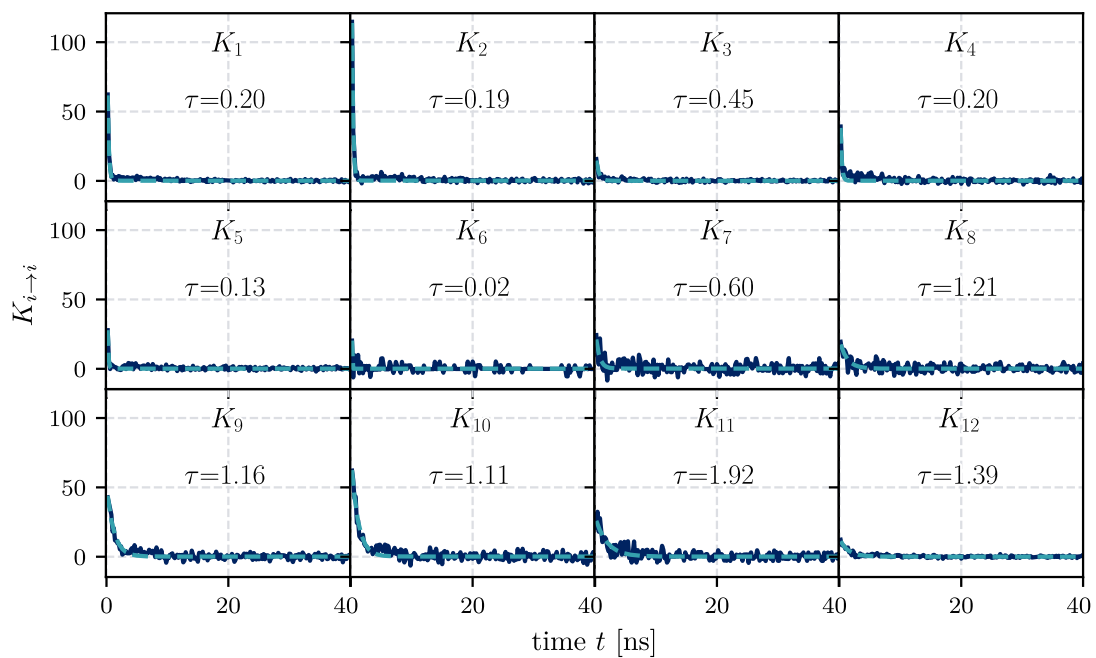


Figure S2: Diagonal element of the qMSM memory kernel for the 300 μ s trajectory of HP35. The kernels are each fit with an exponential function and the decay times estimated from each fit are shown. The kernels obtained from the 30 ns trajectories are quite similar.

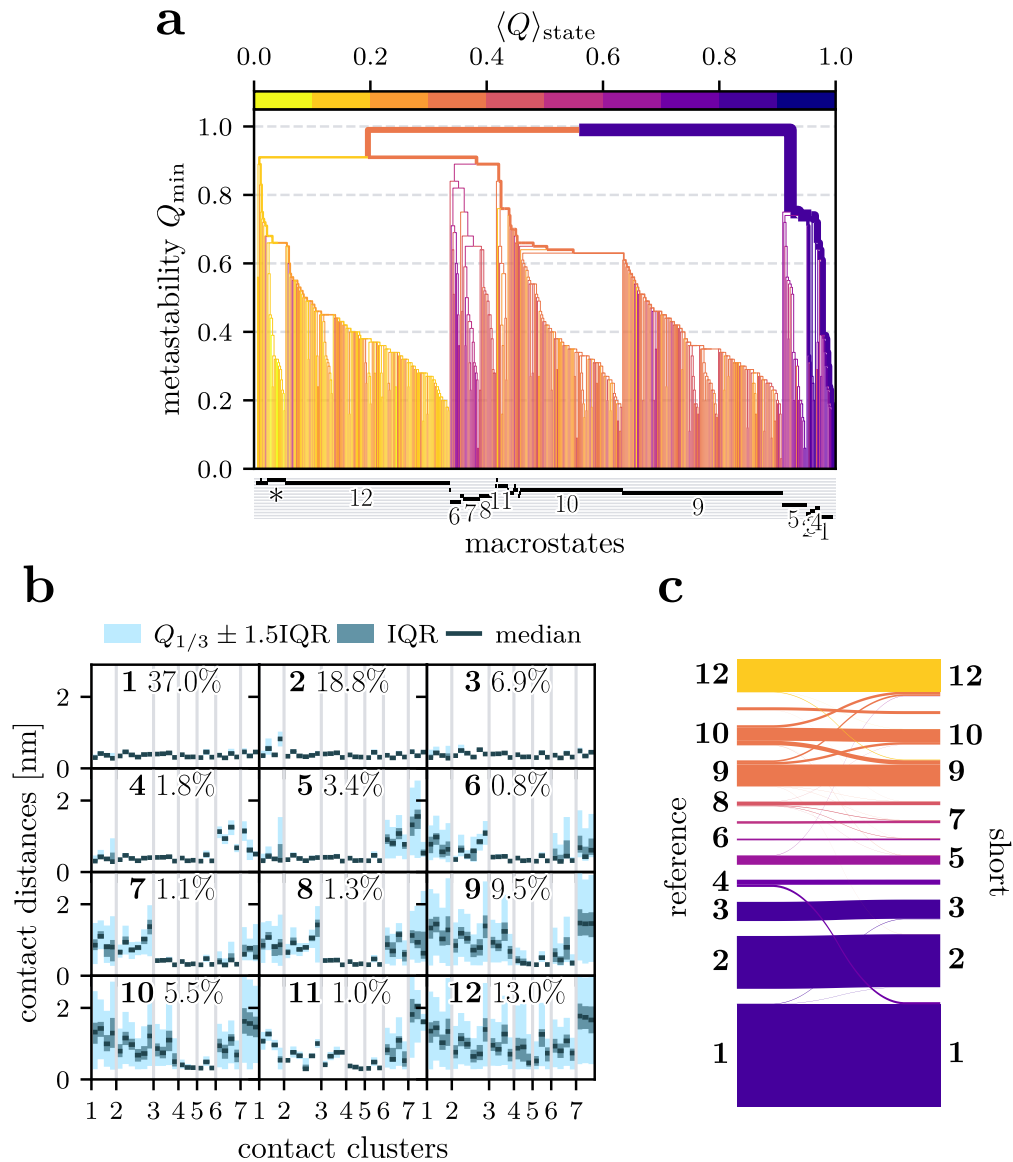


Figure S3: States analysis for the 12 states obtained by lumping the short microstates trajectories as described in Sect. III.B of the main paper. (a) MPP dendrogram^{S1} demonstrating the classification of microstates into metastable states, (b) the contact representation of the resulting metastable states, (c) a Sankey diagram contrasting the states of the reference model^{S2} on the left and the states from the short trajectories on the right.

References

- (S1) Jain, A.; Stock, G. Identifying metastable states of folding proteins. *J. Chem. Theory Comput.* **2012**, *8*, 3810 – 3819.
- (S2) Nagel, D.; Sartore, S.; Stock, G. Selecting Features for Markov Modeling: A Case Study on HP35. *J. Chem. Theory Comput.* **2023**, *19*, 3391 – 3405.